

The role of HMGA2 in activating the IGFBP2 expression to promote angiogenesis and LUAD metastasis via the PI3K/AKT/VEGFA signaling pathway

Shuai QIAN, Fengping WANG, Wenliang LIAO, Jun LIU*

Department of Clinical Laboratory, The Quzhou Affiliated Hospital of Wenzhou Medical University, Quzhou People's Hospital, Quzhou, China

*Correspondence: mingzaixin@wmu.edu.cn

Received September 7, 2023 / Accepted January 12, 2024

This study investigates the molecular mechanism of HMGA2-mediated regulation of IGFBP2 expression in the PI3K/AKT/VEGFA signaling pathway, which is involved in angiogenesis and LUAD metastasis. Target genes with prognostic implications for LUAD patients were selected using bioinformatics, and previously published literature was referenced to predict the molecular regulatory mechanisms. A549 cells were used for *in vitro* validation. Cell proliferation and viability were assessed using CCK-8 and EdU assays, while cell migration ability was evaluated using Transwell and wound healing assays. Changes in angiogenesis were examined using an angiogenesis assay. The targeted binding of HMGA2 with the IGFBP2 promoter was confirmed through dual luciferase reporter gene experiments and ChIP assays. *In vivo* validation was performed using a xenograft mouse model, and changes in angiogenesis and tumor metastasis were observed using western blot, immunofluorescence, and H&E staining. Bioinformatics analysis revealed that HMGA2 was one of the AAGs that differed between normal individuals and LUAD patients and could serve as a critical mRNA for predicting LUAD prognosis. Results from *in vitro* experiments demonstrated that the expression of the HMGA2 gene was significantly upregulated in LUAD cell lines. Through mediating the expression of IGFBP2, the HMGA2 gene activated the PI3K/AKT/VEGFA signaling pathway, promoting the proliferation, migration, and angiogenesis of A549 cells. *In vivo*, animal experiments further confirmed that HMGA2 facilitated angiogenesis and the development and metastasis of LUAD through mediating IGFBP2 expression and activating the PI3K/AKT/VEGFA signaling pathway. HMGA2 promotes angiogenesis and healthy growth and metastasis of LUAD by activating the PI3K/AKT/VEGFA signaling pathway by mediating IGFBP2 expression.

Key words: HMGA2; IGFBP2; PI3K/AKT/VEGFA signaling pathway; angiogenesis; LUAD metastasis; bioinformatics; A549 cells; xenograft mouse model

Lung adenocarcinoma (LUAD) is one of the most common types of lung cancer worldwide, originating from the transformation of lung alveolar epithelial cells. Due to its lack of obvious early symptoms, it has been a focal point of concern for the World Health Organization. LUAD accounts for over 25% of global cancer-related deaths and is a significant cause of mortality, with a 5-year survival rate of only 18%. In comparison to squamous cell carcinoma and small cell lung cancer, LUAD has a higher propensity for metastasis, excessive proliferation, and immune evasion [1], which is associated with its highly migratory and angiogenic capabilities. Abnormal angiogenesis and excessive vascularization are crucial for the growth and metastasis of LUAD. Neoangiogenesis, or neovascularization, refers to forming a new vascular network through endothelial cell proliferation,

migration, and differentiation from pre-existing blood vessel walls. It is an essential biological process in tumor development closely related to tumor initiation, growth, metastasis, and prognosis. Consequently, LUAD cells continuously promote angiogenesis during their growth and metastatic processes to meet their demands for sustained proliferation, survival, and dissemination, thereby driving their progression [2]. Exploring the mechanisms of neovascularization and metastasis in LUAD can contribute to discovering new preventative and therapeutic approaches, ultimately improving the quality of life and overall survival of LUAD patients.

The PI3K/AKT signaling pathway is an important signaling pathway that regulates a series of physiological processes, including cell growth, proliferation, migration, and



angiogenesis [3, 4]. As an essential member of the vascular endothelial growth factor family, VEGFA is a crucial effector of the PI3K/AKT pathway, activating endothelial cell migration and proliferation and promoting neovascularization [5]. VEGFA has been proven to be overexpressed in many diseases, especially tumors, suggesting its potentially pivotal role in tumor angiogenesis and metastasis [6]. However, how VEGFA is regulated and affects angiogenesis and metastasis of LUAD through the PI3K/AKT signaling pathway remains to be investigated.

High Mobility Group A2 (HMGA2) is a member of the HMGA family associated with the occurrence, development, and metastasis of many tumors [7, 8]. Previous studies have shown that HMGA2 is upregulated in LUAD and is associated with poor patient prognosis [9]. However, the exact impact of HMGA2 on the vascular formation and metastasis mechanisms in LUAD is still unclear. IGFBP2 is a member of the insulin-like growth factor binding protein family, and it is also overexpressed in many tumors, especially in LUAD [10]. Some studies have confirmed that IGFBP2 could regulate angiogenesis through the PI3K/AKT signaling pathway, but the specific mechanism and possible intermediaries are still unclear [11, 12].

To this end, we utilize bioinformatics methods to screen critical genes that may affect the prognosis of LUAD patients from many genes and then further validate their functions and mechanisms through *in vitro* and *in vivo* experiments. The purpose of this study is to investigate how HMGA2 activates the PI3K/AKT/VEGFA signaling pathway by mediating the expression of IGFBP2, thereby promoting neovascularization and the growth and metastasis of LUAD, to provide a new theoretical basis and therapeutic strategies for the treatment of LUAD.

Materials and methods

Bioinformatics methods. A total of 600 transcriptome data samples related to LUAD were downloaded from The Cancer Genome Atlas (TCGA) database (<https://portal.gdc.cancer.gov/>). This dataset comprised 59 normal samples and 541 tumor samples. The “limma” package in R language was utilized for performing differential expression analysis of mRNA. The criteria for the selection of differentially expressed genes were set as $|\text{LogFC}| > 2$ and $p < 0.05$. Subsequently, volcano plots were generated using the ggplot2 package, and heatmaps were constructed using the pheatmap package. Additionally, Venn diagrams were created using the jvenn database (<http://jvenn.toulouse.inra.fr/app/example.html>). Furthermore, the “clusterProfiler”, “org.Hs.eg.db”, “enrichplot”, “DOSE”, and “ggplot2” packages in R language were employed for conducting GO and KEGG pathway analysis [13, 14].

Establishment of a mouse xenotransplantation model. A total of 40 BALB/c nude male mice, aged 4–6 weeks, were raised and purchased from Beijing Vital River Laboratory

Animal Technology Co., Ltd. in Beijing, China. They were subjected to a 24 h light/dark cycle and maintained at 25 °C. After one week of adaptation, the mice were randomly divided into four groups, with 10 animals in each group. A549 cells were inoculated in the logarithmic growth phase with lentivirus using Genechem (Shanghai, China) and diluted to a concentration of 1×10^7 cells/ml with PBS. To establish a xenograft model in mice, 0.1 ml of cell suspension was injected under the armpit of each mouse. Three weeks later, euthanasia was performed on the mice to collect tumors and lung tissues. The lung tissue was fixed with 4% polyformaldehyde (Merck Life Science, 30525-89-4) and embedded in paraffin for further experiments. The tumor tissue was stored in a freezer at -80°C and used to make frozen sections [15]. All experiments involving mice were approved by the Animal Ethics Committee of Quzhou People’s Hospital.

H&E staining. Mouse lung tissue paraffin sections were sequentially immersed in xylene I for 10 min, xylene II for 10 min, absolute ethanol I for 5 min, absolute ethanol II for 5 min, 95% ethanol for 5 min, 90% ethanol for 5 min, 80% ethanol for 5 min, 70% ethanol for 5 min, and finally rinsed with distilled water. After dewaxing and dehydration, the sections were soaked in Harris hematoxylin staining solution for 3–8 min, followed by rinsing with tap water. Differentiation was performed in 1% hydrochloric acid alcohol solution for a few seconds, followed by rinsing with tap water and counterstaining in 0.6% ammonia water solution. The sections were then rinsed with tap water. Subsequently, the sections were stained with eosin for 1–3 min. Dehydration and clearing were carried out by sequentially immersing the sections in 95% ethanol I for 5 min, 95% ethanol II for 5 min, absolute ethanol I for 5 min, absolute ethanol II for 5 min, xylene I for 5 min, and xylene II for 5 min. The sections were removed from xylene, air-dried slightly, and then mounted with neutral resin. The lung tissue sections were examined using a Nikon TE200 microscope, and images were collected and analyzed to assess the pathological features of the lung tissue and record relevant data. All reagents used in the experiments were purchased from Guangzhou Sagong Biotechnology Co., Ltd. (Sangon, Guangzhou, China) [16].

Immunofluorescent staining. The tumor tissue was sliced into 10 μm thin sections using a cryostat. Subsequently, the sections were blocked with 5% goat serum (Boster, C-0005) and incubated for 1 h. PECAM primary antibody from Merck Life Science was added and incubated overnight at 4 °C, followed by a 30 min wash with PBS. Afterward, the sections were incubated with a fluorescent secondary antibody for 1 h. Vascular formation was observed using a fluorescence microscope (model DM2500, Olympus Instruments, Shanghai) [17].

Cell culture. A549 human LUAD cell line, BEAS-2B normal human lung epithelial cells, HCC827 and H1299 human non-small cell lung cancer cell lines were all purchased from ATCC (USA). The cells were divided into 4 groups, each containing 6 cells. They were then cultured in

complete media containing 10% fetal bovine serum (FBS). For A549 cells, the medium used was Ham's F-12K+10% FBS. For HCC827 and H1299 cells, RPMI-1640+10% FBS was used. For BEAS-2B cells, DMEM+10% FBS (Gibco, USA, 11965092, 21127022, 31870074) was used. The cultures were maintained in an incubator at 37°C with 5% CO₂ and saturated humidity.

For cell counting purposes, cells were completely digested using trypsin and then added to a complete culture medium containing 10% FBS to terminate the digestion. A 10 µl cell sample was taken using a Countess cell counter (model AMQAX2000, Invitrogen, USA). The sample was mixed with 10 µl of 0.4% trypan blue, and then 10 µl of the mixture was added to a Countess cell counting chamber (model C10228, Invitrogen, USA) for cell counting. Subsequent experimentation and cell passage were performed based on the counted cell numbers.

For slow virus infection, the cells that were infected need to be seeded into a cell culture dish or a 6-well plate 24 h in advance. The cell density should reach approximately 50% confluence on the day of infection. The target cells and control cells were infected with viral solution carrying the target vector, and after 24 h, the fresh culture medium was replaced and further incubated for 48 h for subsequent experiments. If inhibition of the PI3K/AKT pathway is required, MK-2206 (Shanghai YuanYe Biotechnology, S80038) is added to the culture medium at a final concentration of 10 µmol/l.

The passaged cells were treated with OE-HMGA2, sh-HMGA2, OE-IGFBP2, sh-IGFBP2, and OE-HMGA2+sh-IGFBP2 plasmids or their control groups. The sequences of three sh-HMGA2 were as follows: sh-HMGA2-1: 5'-AGTCCCTCTAAAGCAGCTCAA-3'; sh-HMGA2-2: 5'-AGGAGGAACTGAAGAGACAT-3'; sh-HMGA2-3: 5'-GCCACAACAAGTTGTTTCAGAA-3'. The three sh-IGFBP2 sequences were as follows: sh-IGFBP2-1: 5'-CAACCTCAAACAGTGCAAGAT-3'; sh-IGFBP2-2: 5'-CGTGGACAGCACCATGAACAT-3'; sh-IGFBP2-3: 5'-ACAGTGCAAGATGTCTCTGAA-3'.

The lentiviral vector used was pCDH-CMV-MCS-EF1-GFP+Puro (Changsha Abway Biotech, HG-VMS0751), and the sequence information is shown in Supplementary Figure S1. The shRNA plasmid vector was pLKO.1, and plasmid and lentivirus packaging services were provided by Guangzhou Bioscience Biotechnology (Guangzhou, China). The constructed plasmid with a single luciferase reporter gene was co-transfected with the auxiliary plasmid into 293T cells (ATCC, CRL-3216). After verification, amplification, and purification, packaged lentiviruses were obtained. For slow virus-mediated cell infection, 5×10⁵ cells were inoculated into a 6-well plate. When the confluence of the cells reaches 70–90%, culture medium containing an appropriate amount of packaged lentivirus (MOI=10, working titer approximately 5×10⁶ TU/ml) and 5 µg/ml polybrene (Merck, TR-1003, USA) should be added to the cells for infection. After 4 h of infection, an equal amount of a medium was

added to dilute the polybrene. After 24 h of infection, a medium was changed for a fresh one. After 48 h of infection, the infection using a luciferase reporter gene was observed and a resistance selection was performed using an appropriate concentration of puromycin (A1113803, Gibco, Grand Island, NY, USA) to obtain a stably transfected cell line. Cells surviving in the purine nucleoside medium were collected and the efficiency was verified through RT-qPCR [18].

EdU experiment. The cells were inoculated into 24-well plates and the operations on each group of cells in 3 different wells were performed. 5-ethynyl-2'-deoxyuridine (C0071S) was added to the culture medium at a concentration of 50 µmol/l and incubated in a CO₂ incubator for 2 h. Afterward, the culture medium was removed and the cells were rinsed twice with PBS for 5 min each time. Subsequently, the samples were fixed in a PBS solution containing 4% formaldehyde at room temperature for 30 min, then neutralized excess aldehyde with a 2 mg/ml glycine solution. Finally, the samples were washed with PBS for 5 min, incubated at room temperature with PBS containing 0.5% Triton-X-100 for 15 min, and then washed again with PBS for 5 min.

The samples were incubated at room temperature under light-protected conditions, 100 µl of staining solution was added to each well and incubated for 30 min. After incubation, the staining solution was discarded and Hoechst 33342 staining solution was added to stain the nuclei for 30 min, followed by another 5 min of washing. Using a fluorescence microscope (Leica DM2500, Chengguan Instruments (Shanghai) Co., Ltd.), four fields of view were randomly selected in each sample and the number of positive cells in each field was recorded. The EdU labeling rate (%) was calculated: number of positive cells/number of cells with nuclei × 100%. The experiment was repeated three times each time [19].

CCK-8. The CCK-8 assay kit (C0037, Bi Yun Tian) could be used for evaluating cell proliferation. The cells were inoculated into a 96-well plate and incubated for a suitable period for lentiviral infection. Next, 10 µl of CCK-8 reagent was added to each well and incubated for 1 h. Finally, the absorbance was measured at a wavelength of 450 nm using an enzyme-linked immunosorbent assay (ELISA) analyzer to obtain the results [20].

Scratch experiment. After 24 h of infection by lentivirus, the cells were refreshed and further cultured for 48 h before proceeding to the following experimental procedure. During the scratch experiment, a 200 µl pipette tip was used to draw a line inside the well and the cell debris was washed away with PBS. Then, a culture medium was added, and the images were observed and captured with a microscope. Next, the samples were placed in the incubator for further cultivation. During the experiment, we recorded the initial width of each group's scratches at 0 h, 6 h, 12 h, and 24 h and measured them using ImageJ software [21].

Transwell invasion experiment. The working solution of Matrigel matrix gel with a concentration of approximately

200 µg/ml was prepared in advance (Solarbio, 356234). 100 µl of this liquid was added to the upper chamber of the Transwell and incubated at 37°C in a CO₂ incubator for 30 min to allow the matrix to solidify. The infected cells were inoculated at a density of 5×10⁴/well in the upper chamber of Transwell plates. A serum-free culture medium was used as the upper chamber medium. 650 µl of medium containing 20% FBS was added to the lower chamber and incubated in a cell culture incubator for 24 h. The next day, the upper chamber was removed, the culture medium was drained, washed three times with physiological saline, and gently wiped with a cotton swab. Crystal violet (Solarbio, G1062) was used to stain the samples with for 5 to 10 min, followed by a rinse with physiological saline. Randomly selected fields of view under the microscope were photographed and ImageJ software was used to calculate the number of cells crossing the membrane in each group [22].

In vitro angiogenesis assay. The Matrigel matrix gel was diluted with a 4°C serum-free medium at a volume ratio of 1:9, then added 150 µl/well onto a 24-well plate and incubated under UV light overnight. The culture medium of A549 cells infected with lentivirus from various groups after continuous cultivation for 2 days was collected. After centrifugation, the supernatant was mixed with a fresh complete culture medium at a ratio of 1:1. Then, it was added to a 24-well plate coated with matrix gel, with 3 ml of the mixture to each well. HUVEC cells (ATCC, PCS-100-013) with a density of 5×10⁵ were seeded in the aforementioned 24-well plate. After culturing for 72 h, the formation of new blood vessels, defined as HUVECs surrounding a circular tubular structure, was examined. Finally, photos were taken under a fluorescent microscope and statistical analysis was performed [23].

RT-qPCR. Total RNA from tissues and cells was extracted using Trizol (16096020) from Thermo Fisher Scientific (New York, USA). Reverse mRNA transcription to cDNA was performed using the Reverse Transcription Kit (RR047A) from Japan Macro Image. The reaction system was prepared using the Japan Macrographic SYBR® Premix Ex Taq™ II Kit (DRR081) and loaded into an ABI 7500 real-time fluorescence quantitative PCR instrument (ABI, Foster City, CA, USA). The RT-qPCR reaction was performed according to the following protocol: initial denaturation at 95°C for 10 min, followed by 35 cycles of denaturation at 95°C for 15 s, annealing at 60°C for 30 s, and extension at 72°C for 45 s. We used GAPDH as an internal reference. All RT-qPCR settings included 3 replicates/well, with 3 experimental repetitions. The 2-ΔΔCt could represent the fold change in the target gene expression in the experimental group compared to the control group. The formula was as follows: ΔΔCT = ΔCt experimental - ΔCt control, where ΔCt = Ct target gene - Ct reference gene. When the real-time fluorescence signal intensity exceeded the threshold, the amplification cycle number was calculated. The design of the primer is described in Supplementary Table S1 [24].

Western blot. The cells were digested in RIPA lysis buffer containing 1% protease inhibitor and phosphatase inhibitor (P0013B, Beyotime Biotechnology, Shanghai, China). The BCA assay kit was used to quantify the total protein concentration (A53226, Thermo Fisher Scientific, Rockford, IL, USA). After separation by SDS-PAGE electrophoresis, the protein was transferred onto a PVDF membrane (IPVH85R, Millipore, MA, USA) using the wet transfer method. Blocking was performed with 5% BSA at room temperature for 1 h, and then the membranes were incubated overnight at 4°C with the following primary antibodies: HMGA2, IGFBP2, p-PI3K, PI3K, p-AKT, AKT, VEGFA, VEGFC, FGF2, ANGPT1, and GAPDH. The details of the primary antibodies used were as follows: HMGA2 (ab97276, 1:1000, Abcam), IGFBP2 (ab188200, 1:1000, Abcam), p-PI3K (ab278545, 1:1000, Abcam), PI3K (ab227204, 1:1000, Abcam), p-AKT (ab38449, 1:1000, Abcam), AKT (#9272, 1:1000, CST), VEGFA (ab46154, 1:1000, Abcam), VEGFC (ab83905, 1:1000, Abcam), FGF2 (ab208687, 1:1000, Abcam), ANGPT1 (ab183701, 1:10000, Abcam), and GAPDH (ab181602, 1:10000, Abcam).

The membrane was washed with TBST 3 times, 5 min each, and incubated with HRP-conjugated secondary antibody IgG (ab6721, 1:5000, Abcam) at room temperature for 2 h. Then, the membrane was washed with TBST 3 times, 5 min each, the ECL staining solution was added and a signal was detected with a chemiluminescence analyzer. ImageJ 1.48u software (V1.48, National Institutes of Health, USA) was used for protein quantification analysis, which involved quantitative analysis by calculating the ratio of grayscale values of each protein to the reference GAPDH. The experiment was repeated three times [25].

Dual-luciferase reporter gene experiment. In the experiment of dual-luciferase reporter genes, the promoter region of the IGFBP2 gene was amplified from genomic DNA and subcloned into the pGL4-Basic luciferase reporter vector (Promega, USA). Simultaneously, a mutant expression vector was constructed and subcloned into the pGL4-Basic vector (Promega, USA). The construction of the wild-type (WT) and mutant (MT) constructs was confirmed by sequencing. A transcription factor LHX9 expression plasmid was also constructed. HEK-293T cells were seeded in a 24-well plate at a density of 2.0×10⁵ cells/well and transfected with the transcription factor HMGA2 expression plasmid and IGFBP2 reporter gene plasmid using X-tremeGENE 9 (Roche, USA) at a concentration of 50 ng/well according to the manufacturer's instructions. After 24 h post-transfection, the cells were collected and lysed with a lysis buffer from Promega (USA), and the luciferase enzyme activity was measured using the dual-luciferase reporter analysis system (Promega, USA). The experiment was repeated three times [26].

Chromatin immunoprecipitation (ChIP). ChIP was performed in A549 cells. HUVECs (1×10⁷/ChIP) were cross-linked with 18.5% formaldehyde in 15 cm culture dishes, followed by quenching with glycine. EDTA was used to

stop the reaction and the nuclear envelope was disrupted by sonication. After centrifugation, the supernatant containing chromatin was collected. The chromatin solution was then incubated separately with an anti-HMGA2 antibody (ab97296, Abcam, USA) and an anti-normal rabbit IgG antibody (ab172730, Abcam, USA). Finally, qRT-PCR was performed to detect the promoter of the IGFBP2 gene using the method mentioned above [26].

Statistical analysis. All data were processed using the SPSS 21.0 statistical software. The measurement data was expressed in the form of mean \pm standard deviation. To compare two sets of samples, a t-test was used. One-way analysis of variance should be used for comparing multiple groups of samples. When the p-value was less than 0.05, it was considered that there was a significant difference between the means of the two sample groups.

Results

To identify critical mRNAs influencing the prognosis of LUAD patients, we downloaded the clinical and transcriptomic data of LUAD patients from TCGA website. We used Rstudio software for differential expression analysis, heatmap visualization, and volcano plots, with $|\text{LogFC}| > 2$ and $p < 0.05$ as the filtering criteria. A total of 2,073 differentially expressed genes (DEGs) were identified, including 1,734 upregulated genes and 339 downregulated genes (Figures 1A, 1B). We intersected these differentially expressed genes (DEGs) with angiogenesis-associated genes (AAGs) obtained from the GeneCards database and performed functional enrichment analysis for GO and KEGG pathways (Figure 1C). The results showed that these DEGs were mainly enriched in biological processes such as regulation of vasculature development,

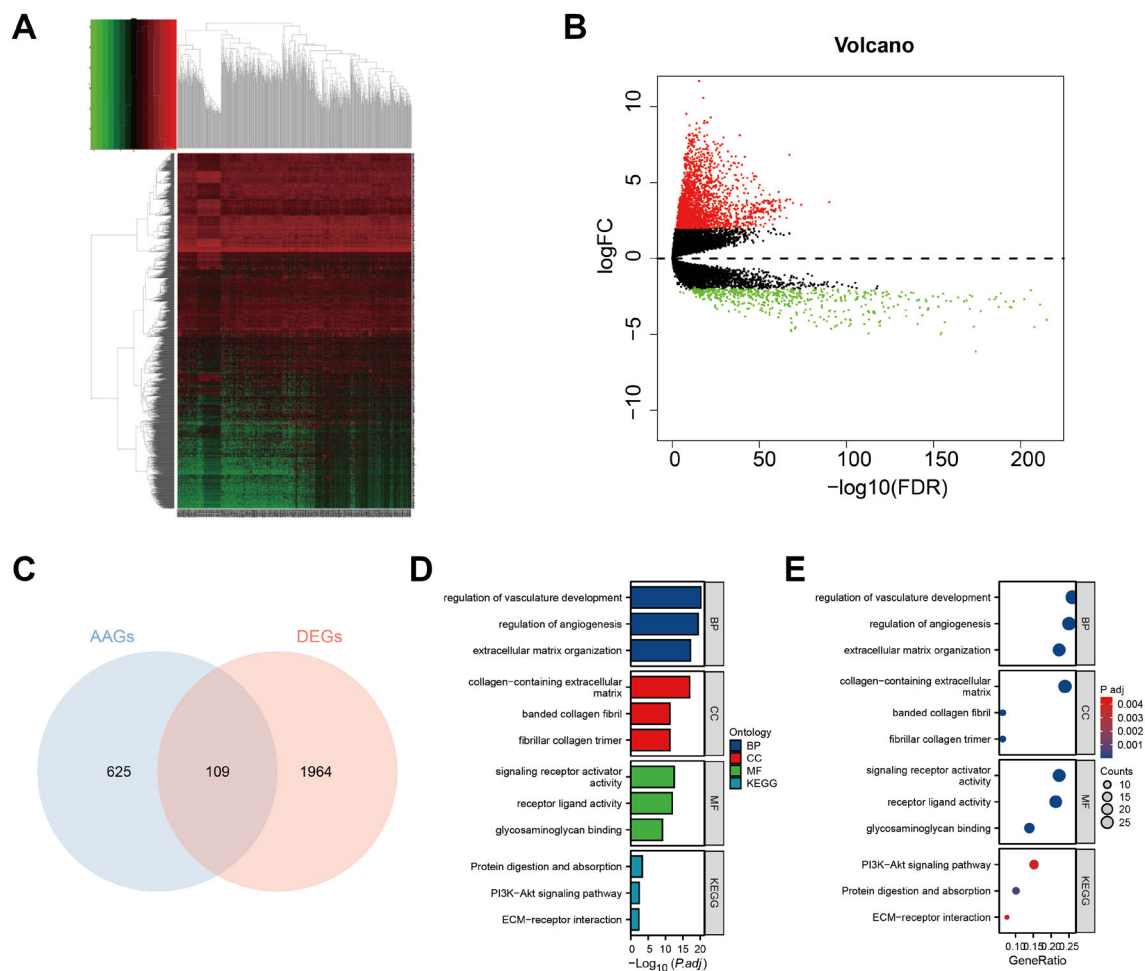


Figure 1. Analysis of bioinformatics to screen differential genes affecting LUAD. **A)** Heatmap of differentially expressed genes (DEGs) between standard control samples (Normal group, n=59) and lung adenocarcinoma (LUAD) patient samples (Cancer group, n=541) in TCGA database, showing the top 10 genes. The red color indicates the upregulation of the gene in the Cancer group, while the blue color indicates the downregulation. **B)** Volcano plot of DEGs between standard control samples (Normal group, n=59) and LUAD patient samples (Cancer group, n=541) in TCGA database. Red dots represent upregulated genes, while blue color represents downregulated genes. **C)** Venn diagram showing the intersection of annotated additional genes (AAGs) and DEGs. **D)** Bar graph showing the results of gene ontology (GO) and Kyoto Encyclopedia of Genes and Genomes (KEGG) enrichment analysis for DEGs. The abbreviations in the figure stand for Biological Process (BP), Cellular Component (CC), and Molecular Function (MF). **E)** Bubble chart representing the results of GO and KEGG enrichment analysis for DEGs.

regulation of angiogenesis, and extracellular matrix organization, as well as signaling pathways such as the PI3K-Akt signaling pathway, Protein digestion and absorption, and ECM-receptor interaction. The above results (Figures 1D, 1E) indicate that these candidate DEGs mainly play roles in angiogenesis and endothelial cell growth.

To further identify key mRNA molecules affecting the prognosis of LUAD patients, we performed univariate Cox analysis on 2,073 DEGs and conducted Lasso risk regression analysis on the obtained results. We plotted the model regression coefficient graph and cross-validation graph (Supplementary Figures S2A, S2B) to select the genes for constructing the Cox model. The results show that the model has the highest accuracy when the number of filtered genes was 19 (the first dotted line on the left of the cross-validation plot). Therefore, we obtained 19 candidate DEGs (GCLC, HCN2, PLEK2, RHOV, INSL4, ADGRE3, TNS4, UNC45B, FCRL5, DLX1, AHSB, FAM83A, HMGA2, PLEKHG4B, ADRB2, GSTA3, CNTNAP2, MFSD6L, GJB3).

We randomly divided the patient samples into train and test groups and utilized the 19 candidate DEGs obtained through joint Lasso analysis to construct a Cox model. The calculation formula was Risk value (HR) = Gene 1 × Gene 1 coefficient + Gene 2 × Gene 2 coefficient + ... + Gene n × Gene n coefficient. Further screening was performed to select 14 candidate Cox-DEGs, which were then visualized using a forest plot (Supplementary Figure S2C). We divided the train and test groups into the high-risk and the low-risk groups based on the risk scores and plotted survival and ROC curves. The survival curves indicate that the survival status of patients in both the training group and the test group align with the expected outcomes of the Cox model (Supplementary Figure S2D). The ROC curve demonstrates that the ROC curve plotted based on risk scores has a good area under the curve (AUC=0.854, AUC=0.629), which could effectively differentiate patients' prognoses (Supplementary Figure S2E). Finally, we plotted risk curves for the train and test groups (Supplementary Figures S2F, S2G), and the results indicated that 14 candidate DEGs were associated with the prognosis of patients. Overall, the Cox model has specific guidance implications for the prognosis assessment of patients with LUAD.

To obtain AAGs associated with LUAD prognosis, we applied the Venn diagram to intersect DEGs, AAGs, and Cox-DEGs. The results indicate that HMGA2 was simultaneously present in all three subsets (Supplementary Figure S2H). We extracted the expression of HMGA2 in LUAD patients and conducted a joint analysis with survival rate. The results showed that the survival rate of patients with low expression of HMGA2 was significantly better than that of patients with high expression (Supplementary Figure S2I). Therefore, we consider HMGA2 a key AAG associated with LUAD prognosis.

***In vitro* cell experiments have shown that HMGA2 was involved in cell proliferation, migration, and angiogenesis.** We used normal human lung epithelial cells (BEAS-2B) as the

control group to select the appropriate cell lines for further experiments. We detected HMGA2 mRNA and protein expression levels in three different LUAD cell lines (A549, HCC827, H1299) using qPCR and western blot techniques. The results showed that HMGA2 mRNA and protein expression levels were highest in the human LUAD cell line A549, so we chose the A549 cell line for subsequent experiments (Figures 2A, 2B). To investigate the effects of HMGA2 on A549 cells, we achieved overexpression and knockdown of HMGA2 by infecting A549 cells with lentiviruses. The results showed that the expression level of HMGA2 mRNA in the OE-HMGA2 group significantly increased, while it decreased in the three sh-HMGA2 groups. We selected the most efficient sh-HMGA2-1 for subsequent experimental validation (Figure 2C).

The deterioration of lung cancer is usually accompanied by excessive proliferation, migration, and invasion of cells [27]. Therefore, we used the CCK-8 method to determine the absorbance of A549 cells infected with lentivirus at 36 h and 72 h at a wavelength of 450 nm. We found that the absorbance of the OE-HMGA2 group was significantly increased compared to the control group at 36 h and 72 h, while the absorbance of the sh-HMGA2 group was significantly decreased (Figure 2D). Next, to investigate whether HMGA2 was involved in regulating proliferation in A549 cells, we used the EdU method to detect cell proliferation after lentiviral infection. The results showed that compared to the control group, the proportion of EdU-positive cells in the OE-HMGA2 group significantly increased, while it decreased in the sh-HMGA2 group (Figure 2E). In addition, we also investigated the regulatory role of HMGA2 on the migration and invasion of A549 cells through the Transwell invasion experiment and scratch assay. The results showed that the number of A549 cells passing through the pores in the OE-HMGA2 group significantly increased while the scratch width significantly decreased. On the other hand, the sh-HMGA2 group showed the opposite effect (Figures 2F, 2G). The above results indicate that HMGA2 has a positive regulatory effect on the proliferation, migration, and invasion of A549 cells.

The occurrence, development, and metastasis of lung cancer were closely associated with angiogenesis. Studies have shown that lung cancer cells activate angiogenesis pathways by infiltrating surrounding tissues and metastasizing to distant sites, thereby promoting tumor growth and metastasis [28]. Therefore, we utilized qPCR and western blot to detect the mRNA and protein expression of angiogenesis-related genes VEGFA, VEGFC, FGF2, and ANGPT1 after HMGA2 overexpression and found a significant increase in their expression. Conversely, the knockdown of HMGA2 resulted in a decrease in their expression (Figures 2H, 2I). We also collected the culture supernatant of different groups of A549 cells after 48 h of cultivation. After centrifugation, the supernatant was mixed with a complete culture medium at a 1:1 ratio for the angiogenesis assay of HUVEC cells. The result shows that the blood vessel length significantly

increased in the OE-HMGA2 group, while it significantly decreased in the sh-HMGA2 group (Figure 2). It indicates that HMGA2 could promote the proliferation, migration, and angiogenesis of A549 cells.

In vitro cell experiments have shown that IGFBP2 was involved in cell proliferation, migration, and angiogenesis. We designed the following experiments to investigate whether IGFBP2 regulates LUAD progression and the

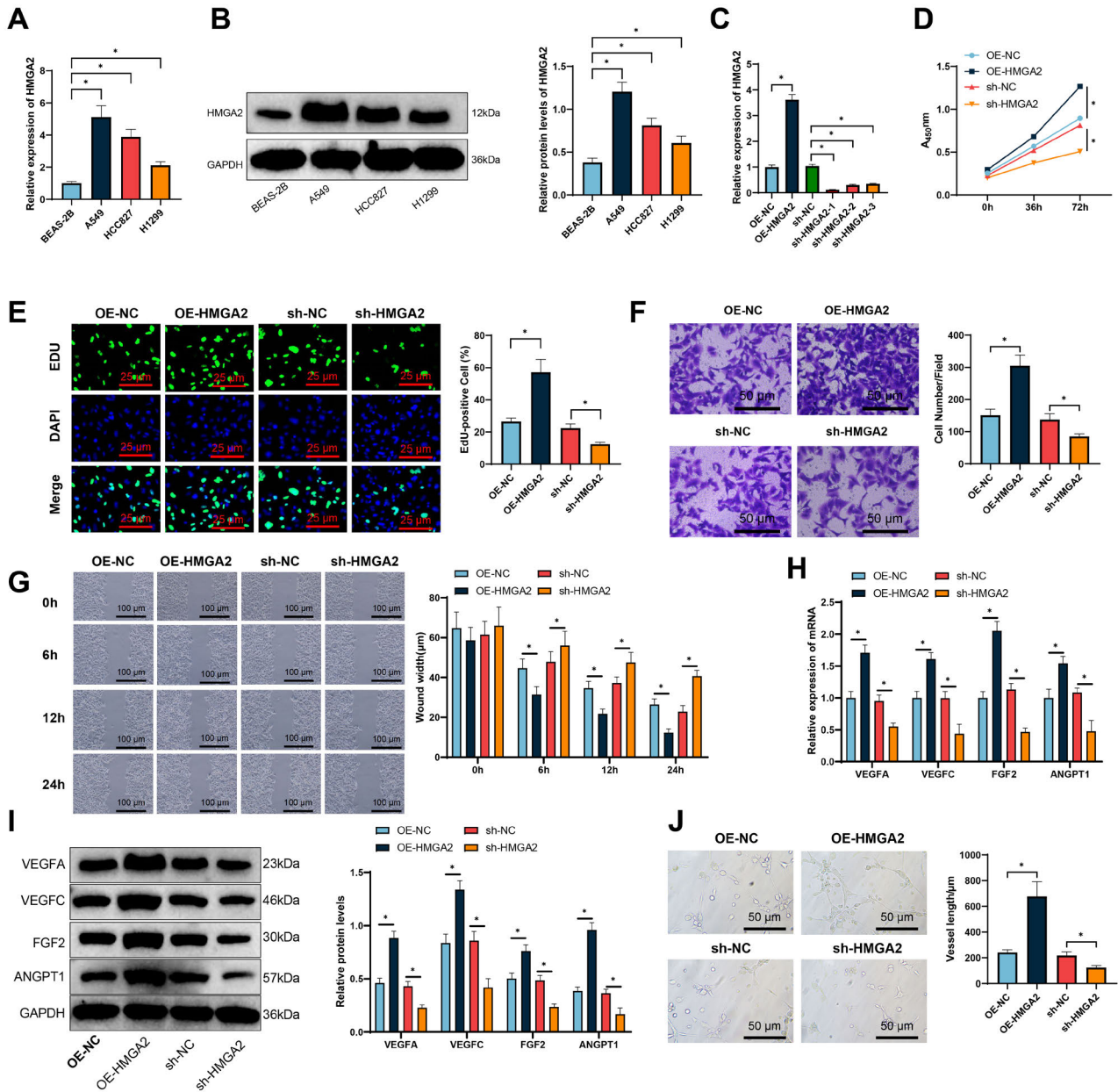


Figure 2. HMGA2 promotes cell proliferation, migration, and angiogenesis. A) mRNA expression levels of HMGA2 in four different cell lines; B) protein expression levels of HMGA2 in four different cell lines with statistical graph; C) efficiency of HMGA2 overexpression and knockdown detection by qPCR; D) proliferation ability of A549 cells transfected with different lentiviruses detected by CCK-8 assay; E) fluorescence images and statistical graph of EdU assay in A549 cells transfected with different lentiviruses, 4 random fields were selected for photography and analysis, scale bar represents 100 μm (200 \times); F) Transwell invasion assay to detect cell invasion ability, scale bar represents 50 μm (400 \times); G) scratch assay to detect cell migration ability, scale bar represents 100 μm (200 \times); H-I) mRNA expression and protein expression changes of angiogenesis-related genes VEGFA, VEGFC, FGF2, and ANGPT1 detected by qPCR and western blot; J) angiogenesis assay to detect angiogenesis in each group and statistical graph, scale bar represents 100 μm (200 \times); Notes: * indicates a significant difference between the two groups with $p < 0.05$, each group had 6 replicate wells for all cells, and the experiment was repeated 3 times; for experiments that required field selection for photography and statistical analysis, 4 random fields were selected for analysis and the average value was used for differential analysis, and subsequent experiments were conducted in the same manner.

potential association between HMGA2 and IGFBP2. First, we achieved overexpression and knockdown of IGFBP2 in A549 cells by transfecting them with lentivirus. We selected the most efficient sh-IGFBP2-1 for subsequent experiments using qPCR detection (Figure 3A). We used the CCK-8 method to measure the absorbance at 450 nm in A549 cells infected with lentivirus at 0 h, 36 h, and 72 h. We found

that the absorbance in the OE-IGFBP2 group was significantly higher than the control group at 36 h and 72 h, while the absorbance in the sh-IGFBP2 group was significantly lower than the control group at 36 h and 72 h (Figure 3B). Through EdU experiments, we found that the proportion of EdU-positive cells in the OE-IGFBP2 group was significantly increased compared to the control group, while the propor-

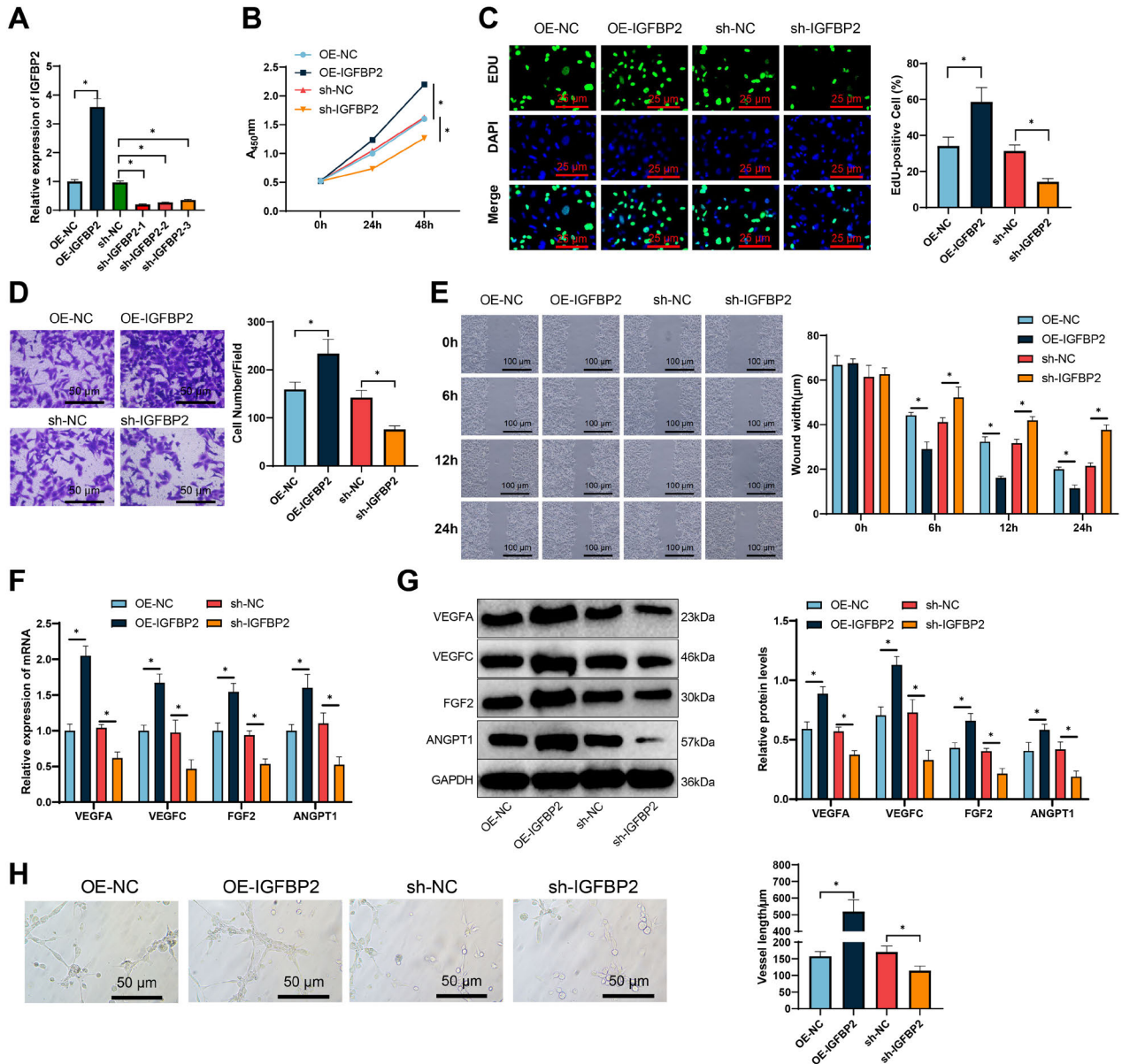


Figure 3. IGFBP2 promotes cell proliferation, migration, and angiogenesis. A) qPCR was used to detect the overexpression and knockdown efficiency of IGFBP2; B) CCK-8 assay was performed to evaluate the proliferation ability of A549 cells transfected with different lentiviruses; C) EdU staining was used to observe the fluorescent images and statistics of A549 cells transfected with different lentiviruses. Scale bar: 100 μm (200×); D) Transwell invasion assay was conducted to assess the invasive ability of cells. Scale bar: 50 μm (400×); E) scratch assay was performed to evaluate the migration ability of cells. Scale bar: 100 μm (200×); F, G) qPCR and western blot were used to measure the mRNA and protein expression changes of angiogenesis-related genes VEGFA, VEGFC, FGF2, and ANGPT1; H) angiogenesis assay was conducted to examine the angiogenesis status of each group, and statistics were generated. Scale bar: 100 μm (200×); Notes: *indicates a significant difference between the two groups with $p < 0.05$. All cell experiments were repeated three times.

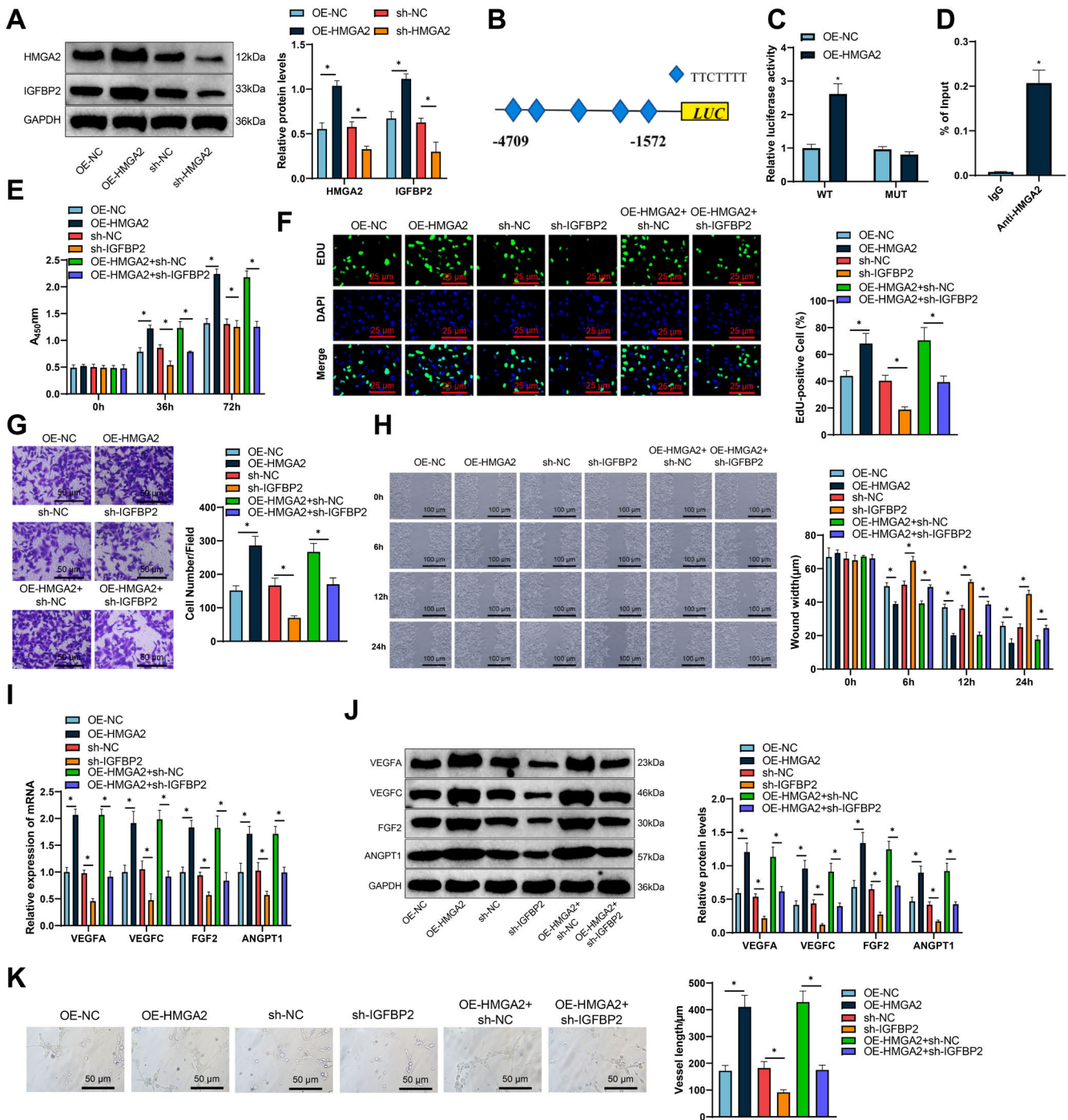


Figure 4. HMGGA2 mediates regulating cell proliferation, migration, and angiogenesis by IGFBP2. A) The protein expression levels were assessed using a western blot, and the corresponding statistical graph was generated. B) A schematic diagram of the IGFBP2 promoter was provided. C) The targeting binding between HMGGA2 and the IGFBP2 promoter was verified using a dual luciferase reporter gene experiment. D) ChIP analysis was conducted to determine whether HMGGA2 directly binds to the IGFBP2 promoter. E) The proliferation ability of A549 cells in each group was examined using CCK-8 assay. F) The fluorescence images and corresponding statistical graph of A549 cells after transfection were obtained using an EdU assay. The scale bar indicates 25 μm (400×). G) Cell invasion capability was assessed using the Transwell invasion assay. The scale bar indicates 50 μm (200×). H) Cell migration ability was evaluated using the scratch assay. The scale bar indicates 100 μm (100×). I, J) The mRNA expression and protein expression changes of VEGFA, VEGFC, FGF2, and ANGPT1, which are associated with angiogenesis, were determined using qPCR and Western blot. K) The angiogenesis of each group was assessed and represented using an angiogenesis assay. The scale bar indicates 50 μm (200×).

tion of EdU-positive cells in the sh-IGFBP2 group was significantly decreased (Figure 3C).

We performed further Transwell invasion experiments to explore the regulation of IGFBP2 on LUAD. The results showed that the number of cells traversing the pores significantly increased after overexpression of IGFBP2, while the number of cells traversing the pores significantly decreased after the knockdown of IGFBP2 (Figure 3D). In the scratch experiment, compared to the control group, the OE-IGFBP2 group showed a significant decrease in scratch width at 6 h, 12 h, and 24 h, while the sh-IGFBP2 group showed the opposite effect (Figure 3E). By using qPCR and western blot, we detected the mRNA and protein expression changes of vascular endothelial growth factor A (VEGFA), vascular endothelial growth factor C (VEGFC), fibroblast growth factor 2 (FGF2), and angiopoietin 1 (ANGPT1) related to angiogenesis. We found that overexpression of IGFBP2 significantly promoted these genes' mRNA and protein expression, while knockdown of IGFBP2 had the opposite effect (Figures 3F, 3G). We also collected the conditioned medium from different groups of A549 cells after 48 h of culture. After centrifugation, the supernatant was mixed with a complete culture medium at a 1:1 ratio and used for the angiogenesis assay of HUVEC cells. The results of the angiogenesis assay showed that, compared to the control group, the vascular length was significantly increased in the OE-IGFBP2 group while significantly reduced in the sh-IGFBP2 group (Figure 3H). The overall results indicate that IGFBP2 could also promote the proliferation, migration, and angiogenesis of A549 cells, similar to the regulatory effect of HMGA2 on A549 cells.

HMGA2 mediates the involvement of IGFBP2 in cell proliferation, migration, and angiogenesis. In previous studies, we have confirmed that HMGA2 and IGFBP2 positively regulate the proliferation, migration, and angiogenesis of A549 cells. Therefore, we could reasonably speculate that HMGA2 may be involved in the proliferation, migration, and promotion of angiogenesis in A549 cells by mediating IGFBP2. To verify this hypothesis, we conducted the following experiments.

When HMGA2 was overexpressed, the expression of IGFBP2 protein increased significantly, while the opposite occurred when HMGA2 was inhibited (Figure 4A). In Figures 4B and 4C, we demonstrated the influence of HMGA2 on the transcriptional activity of the IGFBP2 gene by using the luciferase assay. Additionally, in Figure 4D, we confirmed the binding of HMGA2 to the promoter region of the IGFBP2 gene through ChIP validation. Next, we set up six different treatment groups: OE-NC, OE-HMGA2, sh-NC, sh-IGFBP2, OE-HMGA2+sh-NC, and OE-HMGA2+sh-IGFBP2. The absorbance at 450 nm of A549 cells transfected with OE-HMGA2 was significantly higher than that of the control group at 36 h and 72 h, as detected by the CCK-8 assay.

On the other hand, the absorbance of the sh-IGFBP2 group was significantly lower than that of the control group

at 36 h and 72 h, consistent with the previous experimental results. However, the absorbance of the OE-HMGA2+sh-IGFBP2 group was significantly lower than that of the OE-HMGA2+sh-NC group (Figure 4E). Through EdU experiments, it could be observed that compared to the control group, the proportion of EdU-positive cells significantly increased in the OE-HMGA2 group, while it significantly decreased in the sh-IGFBP2 group. Furthermore, the proportion of EdU-positive cells in the OE-HMGA2+sh-IGFBP2 group also significantly decreased and was comparable to that of the sh-NC group (Figure 4F).

In the Transwell invasion experiment, the cell counts of the OE-HMGA2 group significantly increased, while the cell counts of the sh-IGFBP2 group significantly decreased. The cell counts of the OE-HMGA2+sh-IGFBP2 group also significantly decreased to a level similar to that of the sh-NC group (Figure 4G). In the scratch experiment, the scratching width of the OE-HMGA2 group significantly decreased at 6 h, 12 h, and 24 h. The scratching width of the sh-IGFBP2 group significantly increased at 6 h, 12 h, and 24 h. The scratching width of the OE-HMGA2+sh-IGFBP2 group also significantly increased at 6 h, 12 h, and 24 h, and the width was close to that of the sh-IGFBP2 group (Figure 4H). Changes in mRNA and protein expression of vascular-related genes (VEGFA, VEGFC, FGF2, ANGPT1) were determined by qPCR and western blot. It was observed that the OE-HMGA2 group significantly promoted the mRNA and protein expression of these genes, while the sh-IGFBP2 group had the opposite effect.

Moreover, the OE-HMGA2+sh-IGFBP2 group showed a significant decrease in expression levels, similar to the sh-NC group (Figures 4I, 4J). Similarly, in the angiogenesis assay, the regulation of angiogenesis by each group yielded similar results (Figure 4K). Based on the above experiments, we found that overexpression of HMGA2 could promote the proliferation, migration, and angiogenesis of A549 cells. When HMGA2 was overexpressed while IGFBP2 was knocked down, the favorable regulatory effect of HMGA2 on A549 cells was reversed, and various proliferation, migration, and angiogenesis indicators were similar to the sh-NC group. Indicates that HMGA2 regulates the proliferation, migration, and angiogenesis of A549 cells by mediating IGFBP2.

HMGA2 activates the PI3K/AKT/VEGFA pathway to regulate cell proliferation, migration, and angiogenesis. To verify the hypothesis above, we conducted a western blot analysis to assess the protein expression of the PI3K/AKT/VEGFA signaling pathway. The results revealed that overexpression of HMGA2 led to an upregulation of phosphorylation levels of PI3K and AKT, as well as an increase in VEGFA protein expression. Conversely, when HMGA2 was overexpressed along with IGFBP2 knockdown, we observed a downregulation in the phosphorylation levels of PI3K and AKT, as well as a decrease in VEGFA protein expression. Additionally, in the absence of HMGA2 expression, both the phosphorylation levels of PI3K and AKT, as well as VEGFA

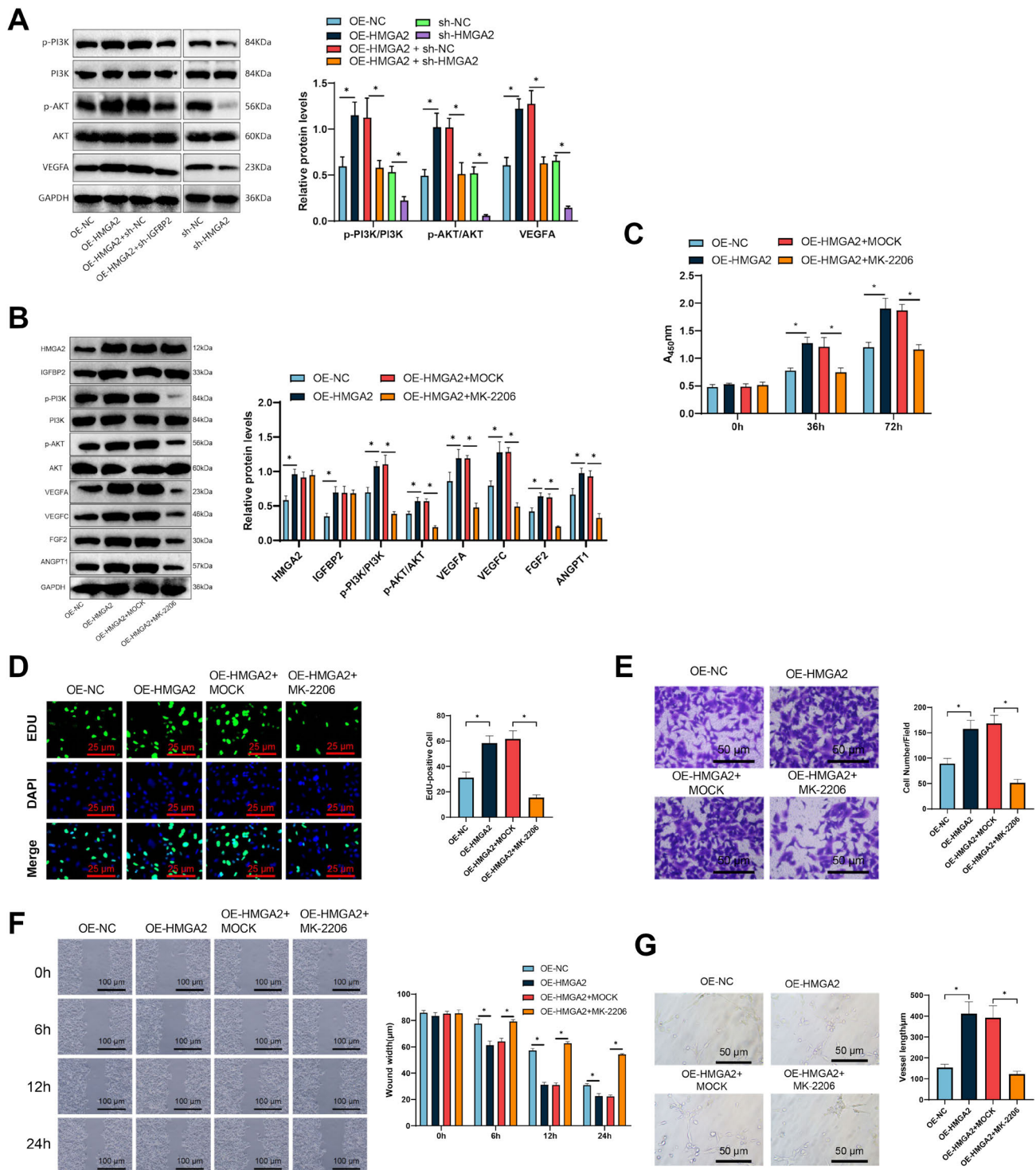


Figure 5. HMGA2 activates the PI3K/AKT/VEGFA pathway to regulate cell proliferation, migration, and angiogenesis. A) Western blot was performed to measure the protein changes in the PI3K/AKT/VEGFA pathway and generate statistics; B) western blot was performed to measure the protein changes in each group and generate statistics; C) CCK-8 assay was conducted to evaluate the proliferation ability of cells; D) EdU staining was used to observe the fluorescent images and statistics of cell proliferation. Scale bar: 100 μm (200 \times); E) Transwell invasion assay was conducted to assess the invasive ability of cells. Scale bar: 50 μm (400 \times); F) scratch assay was performed to evaluate the migration ability of cells. Scale bar: 100 μm (200 \times); G) angiogenesis assay was conducted to examine the angiogenesis status of each group, and statistics were generated. Scale bar: 100 μm (200 \times); Notes: *indicates a significant difference between the two groups with $p < 0.05$. All cell experiments were repeated three times.

protein expression, were downregulated (Figure 5A). Next, we added the PI3K/AKT pathway inhibitor MK-2206 during the cell culture process. The experimental results show that the phosphorylation levels of PI3K and AKT in the OE-HMGA2+MK-2206 group significantly decreased, as well as the protein expression of VEGFA, VEGFC, FGF2, and ANGPT1. However, MK-2206 did not significantly affect the protein expression of HMGA2 and IGFBP2 (Figure 5B).

Through CCK-8 and EdU assays, it was found that the overexpression of HMGA2 significantly increased cell proliferation. However, this effect was significantly reduced in the presence of MK-2206. Meanwhile, Transwell and scratch assays were performed to assess the migration ability of cells. It was found that the invasion and migration ability of cells in the OE-HMGA2+MK-2206 group showed a significant decrease (Figures 5C–5F). Finally, the results of the angiogenesis experiment indicate that overexpression of HMGA2 significantly inhibits the positive regulation of angiogenesis after the addition of MK-2206 (Figure 5G). These experi-

mental results indicate that HMGA2 promotes cell proliferation, migration, and angiogenesis by activating the PI3K/AKT/VEGFA pathway.

Internal experiments have shown that HMGA2 promotes angiogenesis, tumor development, and metastasis. To validate the regulation of HMGA2 on LUAD, we established a xenograft mouse model by injecting logarithmic phase A549 cells into the armpits of mice and subsequently injecting various concentrations of lentivirus through the tail vein. The tumor growth curve shows that overexpression of HMGA2 significantly promotes the volume and weight increase of the tumor. On the contrary, tumor volume and weight were suppressed in the sh-HMGA2 group (Figures 6A, 6B). Through qPCR and western blot analysis of tumor tissue samples, it was found that in the OE-HMGA2 group, compared to the control group, the mRNA and protein expression of HMGA2, IGFBP2, VEGFA, VEGFC, FGF2, and ANGPT1 were significantly increased, and the PI3K/AKT/VEGFA signaling pathway was activated.

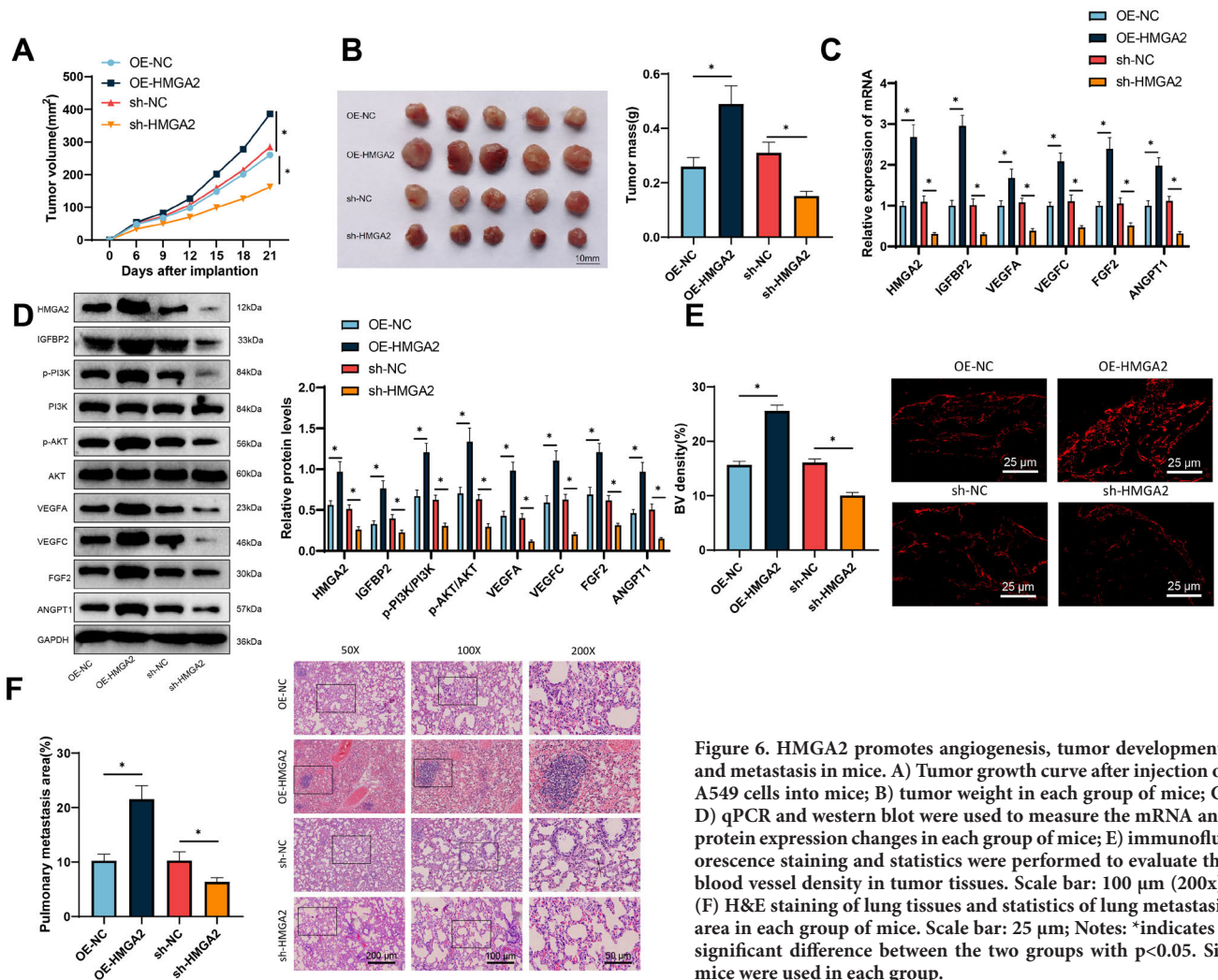


Figure 6. HMGA2 promotes angiogenesis, tumor development, and metastasis in mice. A) Tumor growth curve after injection of A549 cells into mice; B) tumor weight in each group of mice; C, D) qPCR and western blot were used to measure the mRNA and protein expression changes in each group of mice; E) immunofluorescence staining and statistics were performed to evaluate the blood vessel density in tumor tissues. Scale bar: 100 μ m (200x); (F) H&E staining of lung tissues and statistics of lung metastasis area in each group of mice. Scale bar: 25 μ m; Notes: *indicates a significant difference between the two groups with $p < 0.05$. Six mice were used in each group.

In contrast, the results of the sh-HMGA2 group were opposite (Figures 6C, 6D). Immunofluorescence staining of tumor tissues revealed that the OE-HMGA2 group exhibited higher vascular density, while the sh-HMGA2 group showed significantly lower vascular density (Figure 6E). In addition, H&E staining of lung tissues revealed a significant increase in lung metastasis area in the OE-HMGA2 group compared to the OE-NC group, while the lung metastasis area was significantly decreased in the sh-HMGA2 group compared to the sh-NC group (Figure 6F). In summary, the above results indicate that overexpression of HMGA2 promotes the activation of the PI3K/AKT/VEGFA signaling pathway, thereby promoting angiogenesis, tumor growth, and metastasis.

Discussion

LUAD was a common malignant tumor from lung alveolar epithelial cell transformation. The global mortality rate of LUAD accounts for over 25% and is also one of the leading causes of cancer-related deaths worldwide. Compared to squamous cell carcinoma and small cell lung cancer, LUAD was more prone to metastasis, excessive growth, and immune evasion [1, 29]. Abnormal and excessive vascularization was crucial for the growth and metastasis of LUAD because of its highly vascularized nature. During the growth and metastasis of LUAD cancer cells, they promote angiogenesis continuously to meet their needs for continuous proliferation, survival, and metastasis, thus facilitating their further development [2, 30].

This study employed bioinformatics analysis to uncover significant differences in the expression of HMGA2 between normal individuals and LUAD patients. These findings further support the crucial role of HMGA2 in the occurrence and progression of LUAD, which was subsequently validated through *in vitro* and *in vivo* experiments. In the *in vitro* experiments, A549 cells were used, and the results demonstrated that HMGA2 activates the PI3K/AKT/VEGFA signaling pathway by mediating the expression of IGFBP2, thereby promoting cell proliferation, migration, and angiogenesis. These results were further confirmed *in vivo* using a xenograft mouse model. This integrated approach, from computational predictions to laboratory validations, ensures the reliability and practicality of our research outcomes.

HMGA2, a non-histone protein, has been reported to be upregulated in various types of cancers, including LUAD [31]. Studies have shown that HMGA2 plays a role in regulating the development and regulation of non-small cell lung cancer [32]. Additionally, targeting HMGA2 leads to the inhibition of cancer cell proliferation [33]. However, the precise mechanism by which HMGA2 influences angiogenesis and metastasis in LUAD remains uncertain. Our bioinformatics analysis identified HMGA2 as an essential mRNA that influences the prognosis of LUAD patients, which was consistent with previous research. Furthermore, our study

revealed that HMGA2 promotes the proliferation, migration, and angiogenesis of A549 cells, providing a theoretical basis for the impact of HMGA2 on angiogenesis and metastasis in LUAD.

IGFBP2, a member of the insulin-like growth factor-binding protein family, is involved in the regulation and promotion of cancer development and metastasis [34]. Numerous studies indicate a significant elevation of IGFBP2 in the serum or tissue of malignant tumor patients, where it plays a critical role in several vital carcinogenic processes [35]. Some research has confirmed that IGFBP2 regulates angiogenesis through the PI3K/AKT signaling pathway, but its specific mechanism and potential mediators remain unclear. Our results demonstrate that IGFBP2 also promotes the proliferation, migration, and angiogenesis of A549 cells, exhibiting similar regulatory effects to HMGA2. Additionally, some reports suggest that HMGA2 can regulate the expression of IGFBP2. For instance, Wang et al. confirmed through luciferase assays that HMGA2 affects the promoter transcriptional activity of the IGFBP2 gene, thereby regulating its expression [26]. However, to date, there have been few studies reporting on whether HMGA2 regulates the expression of IGFBP2 in LUAD. Therefore, our findings provide a novel perspective in uncovering the role of the HMGA2-IGFBP2 axis in the mechanism of LUAD.

The PI3K/AKT signaling pathway is one of the crucial intracellular signal transduction pathways. It plays a critical role in cells by modulating the activation status of various downstream effector molecules, such as apoptosis inhibition and proliferation promotion. Consequently, this pathway is closely associated with the occurrence and development of various tumors. Studies indicate that the PI3K/AKT signaling pathway plays a significant role in the proliferation, angiogenesis, metastasis, and resistance to radiotherapy and chemotherapy in malignant tumor cells [36], with neoangiogenesis being of paramount importance for tumor growth and metastasis. Our research reveals the molecular mechanism by which HMGA2 activates the PI3K/AKT/VEGFA signaling pathway by mediating IGFBP2 expression, promoting neoangiogenesis, and growth and metastasis of LUAD. This novel finding holds substantial scientific value. Firstly, it provides a new theoretical foundation and research perspective for understanding and investigating the occurrence, development, and metastasis of LUAD. Secondly, the research results uncover the abnormal expression of HMGA2 and IGFBP2 in LUAD and their significant roles in LUAD progression, influencing the search for new targeted therapies for LUAD. Lastly, by delving into the regulatory mechanisms of HMGA2 and IGFBP2, reference may be provided for developing new anticancer strategies.

Based on the above results, we could preliminarily draw the following conclusions: HMGA2 activates the PI3K/AKT/VEGFA signaling pathway by mediating the expression of IGFBP2, which promotes angiogenesis and facilitates the metastasis of LUAD (Supplementary Figure S3). This

study reveals for the first time the molecular mechanism of HMGA2 in promoting angiogenesis, growth, and metastasis of LUAD by activating the PI3K/AKT/VEGFA signaling pathway through mediating expression of IGFBP2. This new finding holds significant scientific value. Firstly, this provides a new theoretical foundation and research perspective for understanding and studying the occurrence, development, and metastasis of LUAD. Furthermore, the research findings also revealed the aberrant expression of HMGA2 and IGFBP2 in LUAD and their crucial roles in developing LUAD, which will have profound implications for the search for new targeted therapies for LUAD. Additionally, an in-depth investigation of the regulatory mechanisms of HMGA2 and IGFBP2 may provide references for developing new anti-cancer strategies.

From a clinical perspective, the expression of HMGA2 and its mediated IGFBP2 may serve as novel biomarkers for the prognosis of LUAD patients. On the one hand, the significant overexpression of these two proteins in LUAD cell lines may be used for early screening and diagnosis. On the other hand, HMGA2 and IGFBP2 play crucial roles in angiogenesis and the development and metastasis of LUAD, indicating their potential as essential targets for targeted therapy.

However, this study also has some limitations. Firstly, our research was conducted only in the A549 cell line and nude mouse models, which may not fully reflect the human body's complex environment and disease states. Furthermore, although we have confirmed the impact of HMGA2-mediated IGFBP2 expression on LUAD, further investigation is needed on other potential regulatory factors and mechanisms of action. In addition, further validation is needed in large-scale clinical trials to explore the application value of HMGA2 and IGFBP2 as novel biomarkers and targets for therapy.

Despite the limitations mentioned above, our study provides an essential foundation for future investigations into the molecular mechanisms of LUAD and the development of novel therapeutic strategies. Firstly, the roles of HMGA2 and IGFBP2 in LUAD and their potential clinical applications need further investigation. In addition, more research must be conducted in multiple LUAD cell lines and models closer to the human body environment to improve the practicality and accuracy of the research. In addition, further investigations are needed to elucidate the specific molecular mechanisms by which HMGA2 mediates the activation of the PI3K/AKT/VEGFA signaling pathway in regulating IGFBP2 expression and to discover novel approaches to inhibit the development of LUAD.

Supplementary information is available in the online version of the paper.

Acknowledgment: This study was supported by the Quzhou Science and Technology Bureau 2023 Guiding Science and Technology Research Project (2023ZD031).

References

- [1] RELI V, TREROTOLA M, GUERRA E, ALBERTI S. Abandoning the Notion of Non-Small Cell Lung Cancer. *Trends Mol Med* 2019; 25: 585–594. <https://doi.org/10.1016/j.mol-med.2019.04.012>
- [2] WEI K, MA Z, YANG F, ZHAO X, JIANG W et al. M2 macrophage-derived exosomes promote lung adenocarcinoma progression by delivering miR-942. *Cancer Lett* 2022; 526: 205–216. <https://doi.org/10.1016/j.canlet.2021.10.045>
- [3] MIRICESCU D, TOTAN A, STANESCU S, II, BADOIU SC, STEFANI C et al. PI3K/AKT/mTOR Signaling Pathway in Breast Cancer: From Molecular Landscape to Clinical Aspects. *Int J Mol Sci* 2020; 22: 173. <https://doi.org/10.3390/ijms22010173>
- [4] KARAMI FATH M, EBRAHIMI M, NOURBAKHS E, ZIA HAZARA A, MIRZAEI A et al. PI3K/Akt/mTOR signaling pathway in cancer stem cells. *Pathol Res Pract* 2022; 237: 154010. <https://doi.org/10.1016/j.prp.2022.154010>
- [5] CLAESSEON-WELSH L, WELSH M. VEGFA and tumour angiogenesis. *J Intern Med* 2013; 273: 114–127. <https://doi.org/10.1111/joim.12019>
- [6] FREZZETTI D, GALLO M, MAIELLO MR, D'ALESSIO A, ESPOSITO C et al. VEGF as a potential target in lung cancer. *Expert Opin Ther Targets* 2017; 21: 959–966. <https://doi.org/10.1080/14728222.2017.1371137>
- [7] MANSOORI B, MOHAMMADI A, DITZEL HJ, DUIJF PHG, KHAZE V et al. HMGA2 as a Critical Regulator in Cancer Development. *Genes (Basel)* 2021; 12: 269. <https://doi.org/10.3390/genes12020269>
- [8] BALZEAU J, MENEZES MR, CAO S, HAGAN JP. The LIN28/let-7 Pathway in Cancer. *Front Genet* 2017; 8: 31. <https://doi.org/10.3389/fgene.2017.00031>
- [9] YU Z, ZHU X, LI Y, LIANG M, LIU M et al. Circ-HMGA2 (hsa_circ_0027446) promotes the metastasis and epithelial-mesenchymal transition of lung adenocarcinoma cells through the miR-1236-3p/ZEB1 axis. *Cell Death Dis* 2021; 12: 313. <https://doi.org/10.1038/s41419-021-03601-2>
- [10] ZHANG B, HONG CQ, LUO YH, WEI LF, LUO Y et al. Prognostic value of IGFBP2 in various cancers: a systematic review and meta-analysis. *Cancer Med* 2022; 11: 3035–3047. <https://doi.org/10.1002/cam4.4680>
- [11] MEHRAN-SHAI R, CHEN CD, SHI T, HORVATH S, NELSON SF et al. Insulin growth factor-binding protein 2 is a candidate biomarker for PTEN status and PI3K/Akt pathway activation in glioblastoma and prostate cancer. *Proc Natl Acad Sci U S A* 2007; 104: 5563–5568. <https://doi.org/10.1073/pnas.0609139104>
- [12] HAN N, FANG HY, JIANG JX, XU Q. Downregulation of microRNA-873 attenuates insulin resistance and myocardial injury in rats with gestational diabetes mellitus by upregulating IGFBP2. *Am J Physiol Endocrinol Metab* 2020; 318: E723–E735. <https://doi.org/10.1152/ajpendo.00555.2018>
- [13] LIANG X, CHENG Z, CHEN X, LI J. Prognosis analysis of necroptosis-related genes in colorectal cancer based on bioinformatic analysis. *Front Genet* 2022; 13: 955424. <https://doi.org/10.3389/fgene.2022.955424>

- [14] DU X, QI H, JI W, LI P, HUA R et al. Construction of a Colorectal Cancer Prognostic Risk Model and Screening of Prognostic Risk Genes Using Machine-Learning Algorithms. *Comput Math Methods Med* 2022; 2022: 9408839. <https://doi.org/10.1155/2022/9408839>
- [15] LIU L, LIU Z, YANG L, WU X, ZHU J et al. Lobetyolin suppressed lung cancer in a mouse model by inhibiting epithelial-mesenchymal transition. *Eur J Histochem* 2022; 66: 3423. <https://doi.org/10.4081/ejh.2022.3423>
- [16] LI Z, GAO M, YANG B, ZHANG H, WANG K et al. Narinigin attenuates MLC phosphorylation and NF-kappaB activation to protect sepsis-induced intestinal injury via RhoA/ROCK pathway. *Biomed Pharmacother* 2018; 103: 50–58. <https://doi.org/10.1016/j.biopha.2018.03.163>
- [17] YANG H, LEE S, LEE S, KIM K, YANG Y et al. Sox17 promotes tumor angiogenesis and destabilizes tumor vessels in mice. *J Clin Invest* 2013; 123: 418–431. <https://doi.org/10.1172/JCI64547>
- [18] LI B, QI ZP, HE DL, CHEN ZH, LIU JY et al. NLRP7 deubiquitination by USP10 promotes tumor progression and tumor-associated macrophage polarization in colorectal cancer. *J Exp Clin Cancer Res* 2021; 40: 126. <https://doi.org/10.1186/s13046-021-01920-y>
- [19] ZENG C, PAN F, JONES LA, LIM MM, GRIFFIN EA et al. Evaluation of 5-ethynyl-2'-deoxyuridine staining as a sensitive and reliable method for studying cell proliferation in the adult nervous system. *Brain Res* 2010; 1319: 21–32. <https://doi.org/10.1016/j.brainres.2009.12.092>
- [20] CHEN L, YANG Y, PENG X, YAN H, ZHANG X et al. Transcription factor YY1 inhibits the expression of THY1 to promote interstitial pulmonary fibrosis by activating the HSF1/miR-214 axis. *Aging (Albany NY)* 2020; 12: 8339–8351. <https://doi.org/10.18632/aging.103142>
- [21] BOBADILLA AVP, AREVALO J, SARRO E, BYRNE HM, MAINI PK et al. In vitro cell migration quantification method for scratch assays. *J R Soc Interface* 2019; 16: 20180709. <https://doi.org/10.1098/rsif.2018.0709>
- [22] YANG Z, JIANG X, ZHANG Z, ZHAO Z, XING W et al. HDAC3-dependent transcriptional repression of FOXA2 regulates FTO/m6A/MYC signaling to contribute to the development of gastric cancer. *Cancer Gene Ther* 2021; 28: 141–155. <https://doi.org/10.1038/s41417-020-0193-8>
- [23] DAI X, XIE Y, DONG M. Cancer-associated fibroblasts derived extracellular vesicles promote angiogenesis of colorectal adenocarcinoma cells through miR-135b-5p/FOXO1 axis. *Cancer Biol Ther* 2022; 23: 76–88. <https://doi.org/10.1080/15384047.2021.2017222>
- [24] WANG C, REN YL, ZHAI J, ZHOU XY, WU J. Down-regulated LAMA4 inhibits oxidative stress-induced apoptosis of retinal ganglion cells through the MAPK signaling pathway in rats with glaucoma. *Cell Cycle* 2019; 18: 932–948. <https://doi.org/10.1080/15384101.2019.1593645>
- [25] YU L, XU H, ZHANG S, CHEN J, YU Z. SDC1 promotes cisplatin resistance in hepatic carcinoma cells via PI3K-AKT pathway. *Hum Cell* 2020; 33: 721–729. <https://doi.org/10.1007/s13577-020-00362-6>
- [26] WANG J, CHEN Y, ZENG Z, FENG R, WANG Q et al. HMGA2 contributes to vascular development and sprouting angiogenesis by promoting IGFBP2 production. *Exp Cell Res* 2021; 408: 112831. <https://doi.org/10.1016/j.yexcr.2021.112831>
- [27] ZHANG C, TANG B, HU J, FANG X, BIAN H et al. Neutrophils correlate with hypoxia microenvironment and promote progression of non-small-cell lung cancer. *Bioengineered* 2021; 12: 8872–8884. <https://doi.org/10.1080/21655979.2021.1987820>
- [28] YANG R, LIU Y, WANG Y, WANG X, CI H et al. Low PRRX1 expression and high ZEB1 expression are significantly correlated with epithelial-mesenchymal transition and tumor angiogenesis in non-small cell lung cancer. *Medicine (Baltimore)* 2021; 100: e24472. <https://doi.org/10.1097/MD.00000000000024472>
- [29] XU F, HUANG X, LI Y, CHEN Y, LIN L. m(6)A-related lncRNAs are potential biomarkers for predicting prognoses and immune responses in patients with LUAD. *Mol Ther Nucleic Acids* 2021; 24: 780–791. <https://doi.org/10.1016/j.omtn.2021.04.003>
- [30] MA Z, CHEN G, CHEN Y, GUO Z, CHAI H et al. MiR-937-3p promotes metastasis and angiogenesis and is activated by MYC in lung adenocarcinoma. *Cancer Cell Int* 2022; 22: 31. <https://doi.org/10.1186/s12935-022-02453-w>
- [31] SAKATA J, HIROSUE A, YOSHIDA R, KAWAHARA K, MATSUOKA Y et al. HMGA2 Contributes to Distant Metastasis and Poor Prognosis by Promoting Angiogenesis in Oral Squamous Cell Carcinoma. *Int J Mol Sci* 2019; 20: 2473. <https://doi.org/10.3390/ijms20102473>
- [32] ARORA S, SINGH P, RAHMANI AH, ALMATROODI SA, DOHARE R et al. Unravelling the Role of miR-20b-5p, CCNB1, HMGA2 and E2F7 in Development and Progression of Non-Small Cell Lung Cancer (NSCLC). *Biology (Basel)* 2020; 9: 201. <https://doi.org/10.3390/biology9080201>
- [33] JIANG C, CAO Y, LEI T, WANG Y, FU J et al. microRNA-363-3p inhibits cell growth and invasion of non-small cell lung cancer by targeting HMGA2. *Mol Med Rep* 2018; 17: 2712–2718. <https://doi.org/10.3892/mmr.2017.8131>
- [34] ANSARI KI, BHAN A, LIU X, CHEN MY, JANDIAL R. Astrocytic IGFBP2 and CHI3L1 in cerebrospinal fluid drive cortical metastasis of HER2+breast cancer. *Clin Exp Metastasis* 2020; 37: 401–412. <https://doi.org/10.1007/s10585-020-10032-4>
- [35] WEI LF, WENG XF, HUANG XC, PENG YH, GUO HP et al. IGFBP2 in cancer: Pathological role and clinical significance (Review). *Oncol Rep* 2021; 45: 427–438. <https://doi.org/10.3892/or.2020.7892>
- [36] ZHU B, ZHOU X. [The study of PI3K/AKT pathway in lung cancer metastasis and drug resistance]. *Zhongguo Fei Ai Za Zhi* 2011; 14: 689–694. <https://doi.org/10.3779/j.issn.1009-3419.2011.08.10>

https://doi.org/10.4149/neo_2024_230907N476

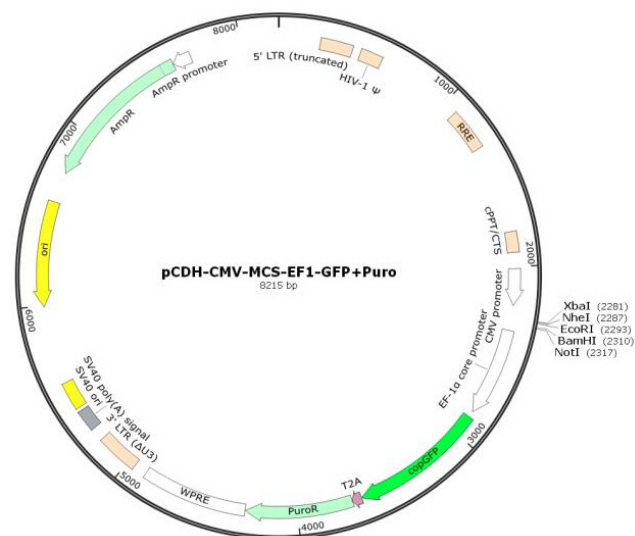
The role of HMGA2 in activating the IGFBP2 expression to promote angiogenesis and LUAD metastasis via the PI3K/AKT/VEGFA signaling pathway

Shuai QIAN, Fengping WANG, Wenliang LIAO, Jun LIU*

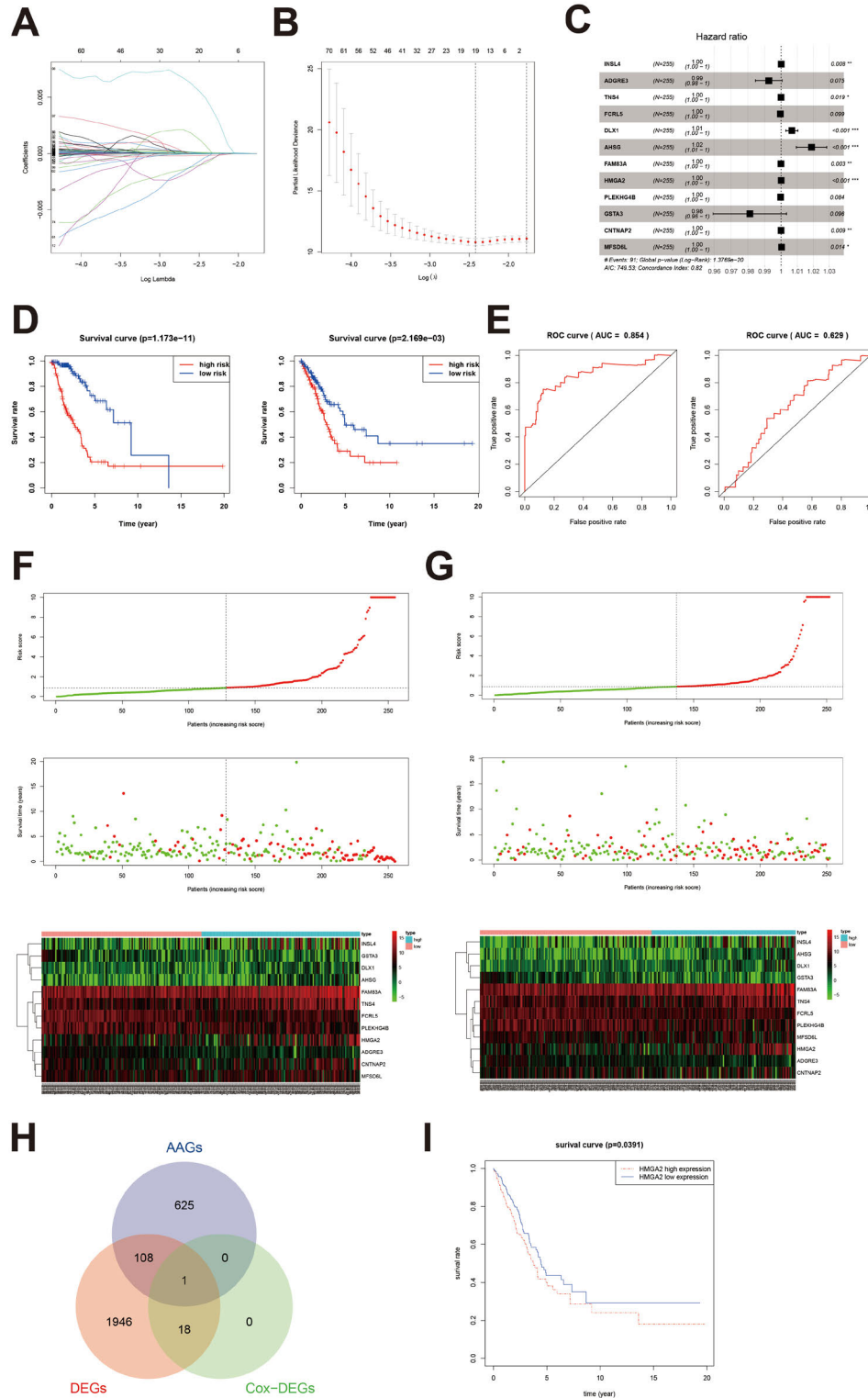
Supplementary Information

Supplementary Table S1. RT-qPCR primer sequence.

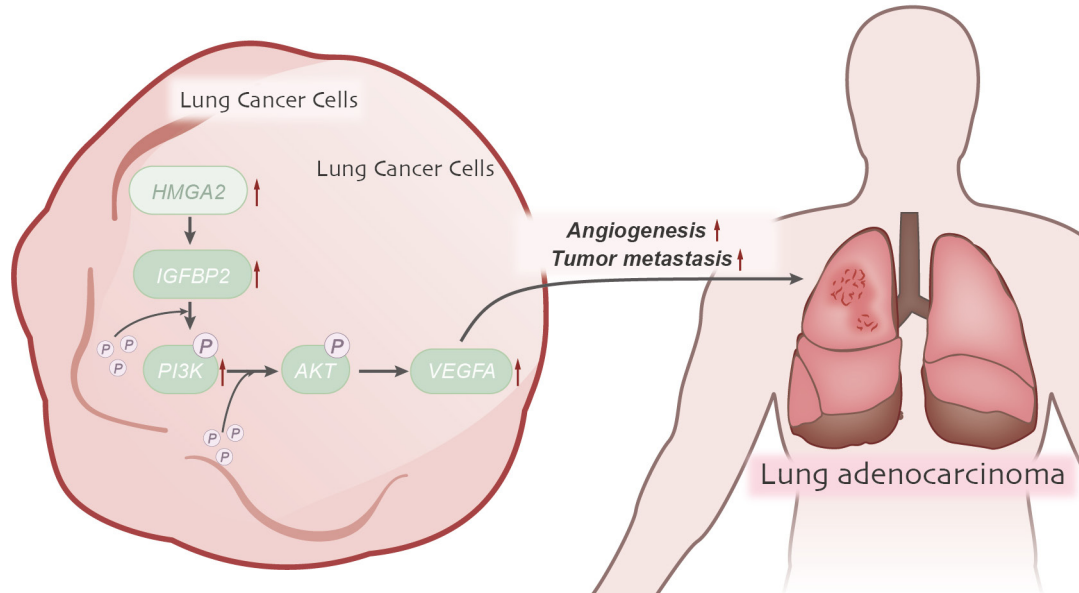
Gene	primer sequence
HMGA2 (human)	Forward: 5'-ACCCAGGGGAAGACCCAAA-3' Reverse: 5'-CCTCTTGGCCGTTTCTCTCCA-3'
IGFBP2(human)	Forward: 5'-GACAATGGCGATGACCACTCA-3' Reverse: 5'-CAGCTCCTTCATACCCGACTT-3'
VEGFA (human)	Forward: 5'-AGGGCAGAATCATCAGGAAAGT-3' Reverse: 5'-AGGGTCTCGATTGGATGGCA-3'
VEGFC (human)	Forward: 5'-GGCTGGCAACATAACAGAGAA-3' Reverse: 5'-CCCCACATCTATACACACCTCC-3'
FGF2 (human)	Forward: 5'-AGTGTGTGCTAACCGTTACCT-3' Reverse: 5'-ACTGCCAGTTCGTTTCAGTG-3'
ANGPT1 (human)	Forward: 5'-AGCGCCGAAGTCCAGAAAAC-3' Reverse: 5'-TACTCTCACGACAGTTGCCAT-3'
GAPDH (human)	Forward: 5'-GGAGCGAGATCCCTCCAAAAT-3' Reverse: 5'-GGCTGTTGTCATACTTCTCATGG-3'



Supplementary Figure S1. Lentiviral vector sequence pCDH-CMV-MCS-EF1-GFP+Puro.



Supplementary Figure S2. Lasso analysis and Cox model to screen prognosis-related genes affecting LUAD. A, B) Lasso regression λ and model regression coefficient plots (A) and cross-validation plots (B) of LUAD patients in the TCGA database; C) Cox model identify genes related to LUAD prognosis; D) Survival curves of high-risk and low-risk groups of patients in the training group and the test group based on the Cox model; E) ROC curves of risk scores in the training group and the test group in the Cox model; F) Risk curve plot of the training group; G) Risk curve plot of the test group; H) Venn diagram showing the intersection of AAGs, DEGs, and Lasso analysis candidate genes; I) Relationship curve between HMGA2 expression and patient survival in TCGA-LUAD data, with 541 patient samples.



Supplementary Figure S3. HMGA2 induces neoangiogenesis and promotes LUAD metastasis by activating the IGFBP2 expression and the PI3K/AKT/VEGFA signaling pathway.